Materials and Design 203 (2021) 109553

Contents lists available at ScienceDirect

Materials and Design

journal homepage: www.elsevier.com/locate/matdes

Silicon-content-dependent microstructures and mechanical behavior of (AlCrTiZrMo)-Si_x-N high-entropy alloy nitride films

Wangying Yu [a], Wei Li [a,*,1], Ping Liu [a], Ke Zhang [a], Fengcang Ma [a], Xiaohong Chen [a], Rui Feng [b], Peter K. Liaw [b]

[a] School of Materials Science and Engineering, University of Shanghai for Science and Technology, Shanghai 200093, PR China
[b] Department of Materials Science and Engineering, The University of Tennessee, Knoxville, TN 37996, USA

HIGHLIGHTS

- The multi-component (AlCrTiZrMo)-Si_x-N high-entropy nanocomposite films with the different Si contents were produced by reactive magnetron sputtering.
- The multi-component (AlCrTiZrMo)-Si_x-N high-entropy nanocomposite films are composed of the structure of nanocrystals encapsulated by the Si_3N_4 interfaces.
- With the addition of Si elements, the (AlCrTiZrMo)-Si_x-N film forms a nanocomposite structure, and the mechanical properties are improved.

GRAPHICAL ABSTRACT

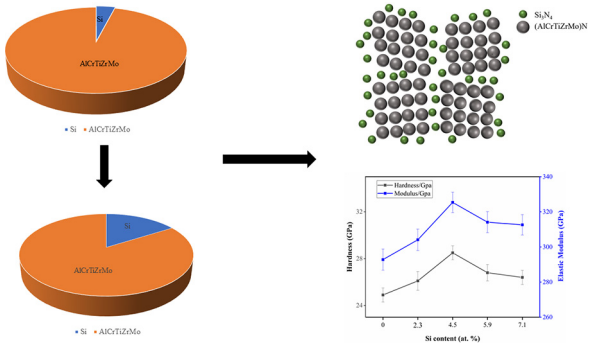

ARTICLE INFO

Article history:
Received 21 September 2020
Received in revised form 2 February 2021
Accepted 2 February 2021
Available online 5 February 2021

Keywords:
(AlCrTiZrMo)-Si_x-N films
Microstructure
Mechanical property
Nanocomposite structure

ABSTRACT

The multi-component (AlCrTiZrMo)-Si_x-N high-entropy films with different silicon contents were deposited on the silicon substrate by magnetron sputtering. The influence of silicon contents on the structures and properties of the films was studied by means of X-ray diffraction (XRD), scanning electron microscopy (SEM), high-resolution transmission electron microscopy (HRTEM), electron probe microanalyzer (EPMA) and nanoindentation. The results show that the (AlCrTiZrMo)N film without silicon has columnar crystals and the (200)-preferred direction. With the increase of the silicon content, the films gradually change from columnar grains with a (200) preferential orientation to structures with amorphous phases (amorphous phases are the state of near order and long disorder in the arrangement of atoms in a solid state) containing nanocrystals (nanocrystallites are single-phase (AlCrTiZrMo)N of grains with a size of 5–10 nm) with finer grains. As the silicon content increases, the mechanical properties of the films first increase then decrease. Thus, when the silicon content is 4.5 atomic percent (at.%), the film obtained possessed comprehensive mechanical properties with the maximum hardness and modulus values of 28.5 GPa and 325.4 GPa, respectively. The results show that the improvement of hardness and modulus is mainly attributed to the microstructures of the films.

1. Introduction

Hard films, including nitride films, carbide films, oxide films, etc., with high hardness, great wear resistance, corrosion resistance, are widely used in the cutting industry [1–4]. Along with the rapid development of the machining industry, the traditional single-metal compound

* Corresponding author.
E-mail address: liwei176@usst.edu.cn (W. Li).
[1] Corresponding author. Doctor, Prof. School of Materials Science and Engineering, University of Shanghai for Science and Technology, Shanghai, 200093, China.

https://doi.org/10.1016/j.matdes.2021.109553

hard film has been unable to satisfy the use of some tools in harsh environments. Therefore, new films with higher hardness, greater wear resistance are urgently needed to be explored. Binary system films (TiN and CrN) [5,6], ternary films (CrAlN) [7], multilayer films (TiC/VC and TiAlN/CrN) [8,9], and so on have been gradually studied and applied in large quantities. In 2004, Yeh et al. and Cantor et al. broke the traditional design concept and proposed the concept of high-entropy alloys (HEAs) or equiatomic multicomponent alloys (EMAs) [10,11]. HEAs are composed of at least five major metal elements, each with concentrations ranging from 5 atomic percent (5 at.%) to 35 at.% [12–14].

Compared to traditional hard films, the composition of HEAs locates closer to the center of the compositional space, which provides HEAs with many attractive properties, such as higher hardness, greater wear resistance, fatigue, corrosion, irradiation resistance, superconductivity, and high catalytic activity [15–27]. Due to the high entropy of mixing, slow diffusion, and severe lattice distortion, HEAs are more likely to form face-centered-cubic (FCC), body-centered-cubic (BCC), and hexagonal-close-packed (HCP) structures than intermetallic compounds [28–31]. For the first time, Chen et al. prepared two kinds of HEA films using AlCoCrCuFeMnNi and $Al_{0.5}$CoCrCuFeNi multi-principal HEA targets. Their results showed that the microstructure of HEA film was a single FCC structure or a mixture of FCC and BCC phases [32]. Cui et al. studied the effects of different N_2 flows on the microstructures and mechanical properties of (AlCrTiZrHf)N films [33]. The results showed that the AlCrTiZrHf HEA films were amorphous. With the increase of the N_2 flow rate, the AlCrTiZrHf HEA nitriding film was transformed into an FCC structure. With the development of the research, it is found that the HEA, the HEA nitrides, and so on have better properties than those of traditional nitrides [31,34–38].

The hard film has good mechanical properties with a proper amount of silicon [39]. In order to study the mechanism of the performance optimization of multi-component films, many researchers have studied the films prepared with different silicon contents. Li et al., in 1992, prepared TiSiN nanocomposite films using a physical vapor deposition (PVD) technology, and the results showed that the film had the ultra-high hardness [40]. The appearance of high-hardness films has aroused the interest of many researchers on their hardening mechanisms. In 1995, Veprek and his co-workers did a great amount of research and proposed nanocomposite films composed of nc-TiN and a-Si_3N_4 (nc for nanocrystalline, and a for amorphous) [41]. At present, this model is widely accepted internationally. Shi et al. prepared the nanocomposite Ti-Al-Si-Cu-N film on the substrate of a high-speed steel by the vacuum cathode arc ion plating (AIP) technology, and systematically studied the effect of the silicon content on the microstructures and properties of the film [42]. The results show that TiAlSiCuN films are nanocomposite materials, which are composed of TiAlN and Cu in the nanoscale state and Si_3N_4 in the amorphous state. Niu et al. prepared (AlCrTiZrV)-Si_x-N films with different silicon contents by the magnetron-sputtering technology, and investigated the influence of the silicon content on the microstructures of the films [43]. Thus, the proper silicon content can refine the grain, change the microstructure, and optimize the mechanical properties of the film.

Metal Mo is easy to react with N element to form MoN, which has high melting point and hardness, good thermal stability. At present, there are few studies on the AlCrTiZrMo HEA nitride films. Therefore, in this study, an AlCrTiZrMo HEA target was used as the experimental material, and the method of direct current (DC) magnetron sputtering was adopted to systematically prepare (AlCrTiZrMo)-Si_x-N films with different silicon contents and conduct a series of characterization of the films, so as to study the influence of the Si content on the microstructures and mechanical properties of (AlCrTiZrMo)-Si_x-N films.

2. Experimental

2.1. Film preparation

The (AlCrTiZrMo)-Si_x-N HEA nitride films were deposited on a silicon substrate (35 mm × 25 mm × 0.5 mm) by a JPG-450 multi-target magnetron sputtering system with single magnetron, using an AlCrTiZrMo target with a thickness of 3 mm and a diameter of 75 mm. The making process of the AlCrTiZrMoSi composite target can be outlined as follows: with the low-speed wire electrical discharge machine (EDM), the single-crystal Si target and the five HEA targets with equal molar contents were cut off successively, and 4 pieces of 25 equally divided small fan-shaped plates. Then, 84% of the HEA was kept unchanged. By changing the number of Si segments, composite targets with $V_{Si}/V_{AlCrTiZrMoSi}$ of 4%, 8%, 12%, and 16% were assembled as Fig. 1.

The experimental steps are presented as follows: after polishing, the monocrystalline silicon matrix at the mirror level was cleaned in alcohol and acetone by the 80 kHz ultrasonic for 15 min, followed by ion cleaning. The base pressure was pumped down to 3.0×10^{-4} Pa before the deposition. During the deposition, the Ar and N_2 flow rates were both controlled to be 10 standard cubic centimeter per minute (sccm). When the film is deposited, the working pressure is adjusted to 0.7 pa, and the sputtering power of the DC power supply is 180 W. Besides, the substrate is controlled by the computer software to rotate at the speed of 0.5 rps (revolution per second), so that the thin film can grow uniformly. The deposition time of the film was 1.5 h. The details of deposition parameters of nitride films of (AlCrTiZrMo)-Si_x-N are presented in Table 1.

2.2. Film characterization and measurement

The crystalline structure and phase analyses were characterized by the D8 Advance X-ray diffractometer (XRD, Bruker, Germany) using the CuK_α radiation ($\lambda = 0.15406$ nm). The bonding structure in the films was characterized by a high-resolution X-ray photoelectron spectrometer (XPS, ESCALAB250, Thermo). Quanta FEG450 field emission environmental electron microscope (SEM, FEI, USA) and a Tecnai $G^2$20 high-resolution field-emission transmission electron microscope (HRTEM, FEI, USA) can be used to observe and analyze the microstructures of the films. The elemental distributions of the films were characterized by the electron probe microanalyzer (EPMA, JXA-8530F PLUS). The mechanical properties of the films can be measured by the NANO

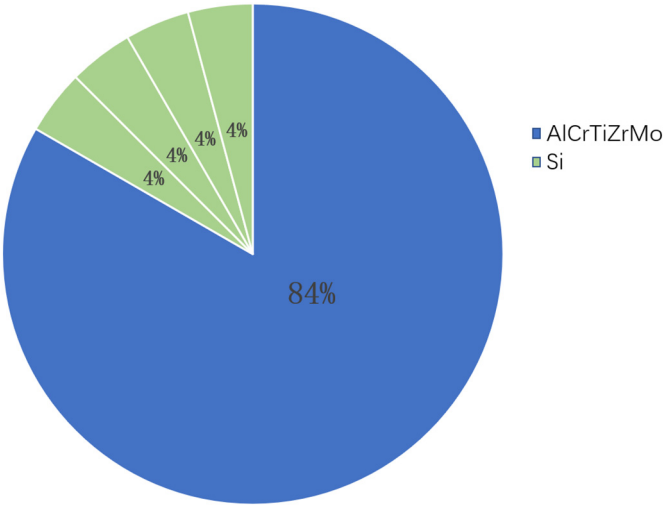

Fig. 1. Schematic illustration of the AlCrTiZrMoSi_x composite target.

Table 1
Deposition parameters (the substrate-to-target distance d_{s-t}, the substrate bias Us, the deposition rate aD, the elastic recovery We, and so on) of nitride films of (AlCrTiZrMo)-Si_x-N.

P	d_{s-t}	Us	We	Ts	h	aD	$V_{Si}/V_{AlCrTiZrMoSi}$	Si
[W]	[mm]				[nm]	[nm/min]		[at.%]
180	60	0	50	room temperature	1597	18	0	0
180	60	0	54	room temperature	3590	40	4%	2.3
180	60	0	63	room temperature	3520	39	8%	4.5
180	60	0	60	room temperature	1422	16	12%	5.9
180	60	0	58	room temperature	2448	27	16%	7.1

instrument, a G200 nano indenter (Agilent, USA) with the Berkovich indenter. The load-unload curves were obtained by accurately recording the change of the loading depth with the load. The hardness and elastic modulus were calculated by the Oliver–Pharr model [44]. During the measurement, the loading depth was less than 1/10 of the thickness of the films to eliminate the effect of the substrate on the measurements. Each hardness or elastic modulus value was an average of at least 16 measurements.

3. Results

3.1. Effect of Si content on microstructures of AlCrTiZrMo-Si_x-N films

The variation trends of the (AlCrTiZrMo)-Si_x-N films with different Si contents are presented in Fig. 2. From Fig. 2, it can be found the O content, around 5 at.%, changed little in the films, when the Si content increases. This may be attributed to the residual oxygen in the equipment involved in the reaction when preparing the films. With the incorporation of Si, the silicon content in the HEA-nitride film also increases gradually, indicating that the silicon element can be successfully doped into the nitride film as expected. There is almost no difference in the compositions of metal atoms in the HEA-nitride films, which indicates that the target material is close to the equal molar ratios of various elements. The contents of metals in the films slightly decrease, which may be due to the increase of volume of silicon in the target and the formation of nitride in the films.

Fig. 3 shows the XRD patterns of the (AlCrTiZrMo)-Si_x-N films with different silicon contents. Without the Si element, the (AlCrTiZrMo)N film presents a simple FCC structure with the diffraction peak near $2\theta = 42°$, which corresponds to the (200) crystal planes. From the figure, it can be inferred that the (AlCrTiZrMo)N film is a solid-solution nitride composed of binary nitrides of the five elements of Al, Cr, Ti, Zr, and Mo. This feature indicates that a solid-solution phase of the FCC structure is formed in the (AlCrTiZrMo)N films, with good crystallinity, and no other complex intermetallic compounds in the film. The high-

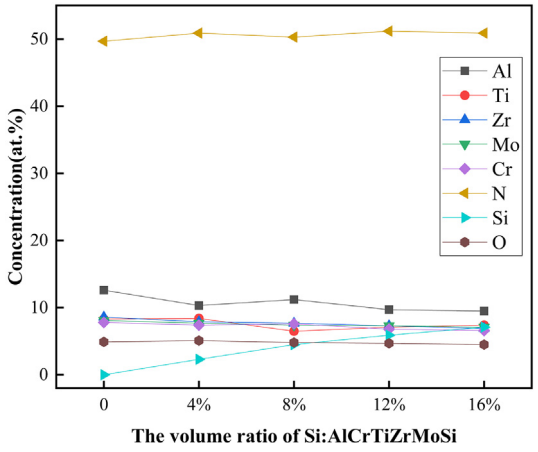

Fig. 2. Trends of AlCrTiZrMo-Si_x-N thin-film elements with different Si contents.

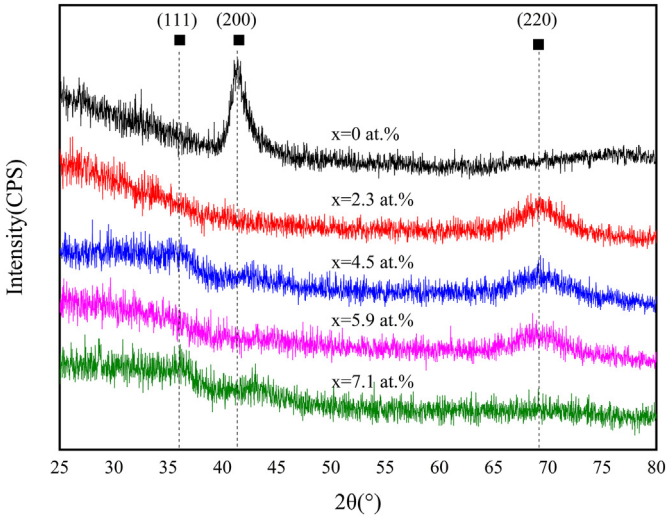

Fig. 3. XRD patterns of AlCrTiZrMo-Si_x-N films with different Si contents.

entropy effect of HEAs is the main reason for this phenomenon. When the mixing entropy of the multi-component system is greater than the mixing entropy required to form intermetallic compounds, the formation of intermetallic compounds will be inhibited, which makes HEAs tend to form a stable solid-solution crystal structure [45–47]. With the addition of Si elements, there aren't significant diffraction peaks observed at $2\theta = 42°$ in (AlCrTiZrMo)-Si_x-N films, indicating that the (200) diffraction peaks of the films disappeared with the increase of Si. Meanwhile, the Si_3N_4 phases are not observed in the XRD spectra, which implied that the interface phase content was very low in (AlCrTiZrMo)-Si_x-N film. Compared with (AlCrTiZrMo)N, it can be seen that for the (AlCrTiZrMo)-Si_x-N (x = 2.3 at.%, 4.5 at.%, 5.9 at.%, and 7.1 at.%) films mixed with Si elements, the XRD diffraction patterns show low-intensity diffraction peaks at about $2\theta = 35°$ and $2\theta = 69°$, respectively, corresponding to the (111) and (220) peaks of the FCC structure.

According to the Eq. (1), the crystallinity of the films can be calculated roughly using origin software, which decreased from 22.5% of (AlCrTiZrMo)N to 12.8% of (AlCrTiZrMo)-$Si_{5.9}$-N. When the silicon content is 7.1 at.%, there is no obvious diffraction peaks. This result indicates that with the addition and increase of Si elements, compared with the (AlCrTiZrMo)N films, the crystallinity of the films decreases, and the microstructure is nanocrystalline or amorphous.

$$\text{Crystallinity} = \frac{\text{Area of crystalline peaks}}{\text{Area of all peaks (crystalline + Amorphous)}} \times 100\% \quad (1)$$

The XPS analysis of Si 2p spectra for (AlCrTiZrMo)-Si_x-N shown in Fig. 4. Analysis of the binding energy from Si 2p peak, the high-intensity peaks at 101.8 eV can be assigned to Si–N bonds in the Si_3N_4, indicating that silicon represented as nitride state of Si_3N_4 in AlCrTiZrMo)-Si_x-N films [30,42]. As the silicon content increases, the

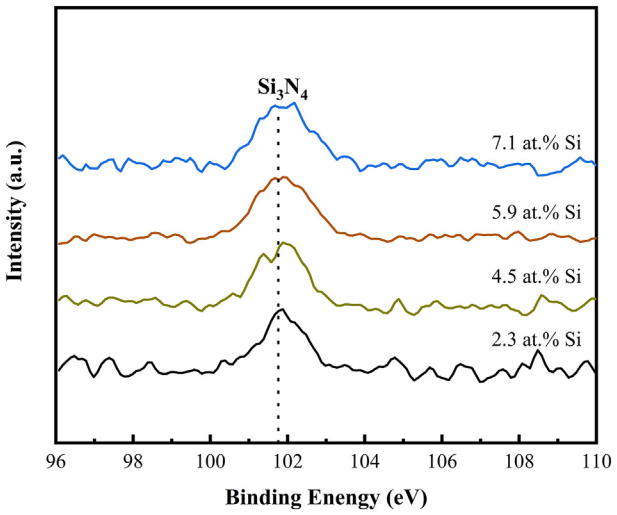

Fig. 4. XPS spectra of Si 2P of AlCrTiZrMo-Si_x-N films with different Si contents.

content of Si_3N_4 is increasing, implying the thickness of amorphous boundary phase increases. Combined with the results of XRD analysis, the structure with amorphous phases Si_3N_4 containing nanocrystals is presented in the films.

Fig. 5 shows the SEM morphologies of the cross sections of (AlCrTiZrMo)-Si_x-N films with different Si contents. As can be seen from the figure, the films have a good combination with the substrate, without the obvious interface and void, and the surface and internal quality of the films are good, and no obvious impurities and defects have been found. From Fig. 5a, the (AlCrTiZrMo)N film without silicon contains clear columnar crystals. However, there are dense structures with no obvious columnar crystal growth characteristics in Figs. 5b, c, d, and e. This result is attributed to the addition of the silicon content.

The cross-sectional images of the (AlCrTiZrMo)N and (AlCrTiZrMo)-$Si_{4.5}$-N film under the low power HRTEM are shown in Fig. 6. According to Fig. 6a, the (AlCrTiZrMo)N film grows in columnar crystals. From Fig. 6b, the (AlCrTiZrMo)-$Si_{4.5}$-N film has no obvious columnar crystal-growth characteristics. Meanwhile, the film has a very dense and smooth cross-sectional structure and becomes denser without visible particle characteristics. This trend demonstrates that the film has finer grains.

The HRTEM and selected electron diffraction (SAED) images of (AlCrTiZrMo)N films and (AlCrTiZrMo)-$Si_{4.5}$-N films cross sections are shown in Fig. 7. It can be seen from Fig. 7a that under the high HRTEM, the grains of (AlCrTiZrMo)N thin films (represented by letters, A, B, C, D) are coarse and can reach tens of nanometers in size. There is no other phase between the different grains, which are in the direct contact with each other. Fig. 7b shows that the grains (yellow-dotted lines) of the (AlCrTiZrMo)-$Si_{4.5}$-N film are refined, which can reach 5 nm. This feature indicates that the grain size reaches the nanocrystalline level, which also confirms the above results of the XRD analysis. With the addition of Si elements, the grain size of the thin film becomes small and can reach the nanocrystalline level. The addition of Si elements can effectively refine the grain size. Moreover, it can be seen from Fig. 7b that at the high-power HRTEM, the grains of (AlCrTiZrMo)-$Si_{4.5}$-N thin films (inside the yellow dashed line) do not directly contact, and there is an obvious reticular interfacial phase between the grains, without orderly lattice structures. It can be speculated that the interfacial phase is

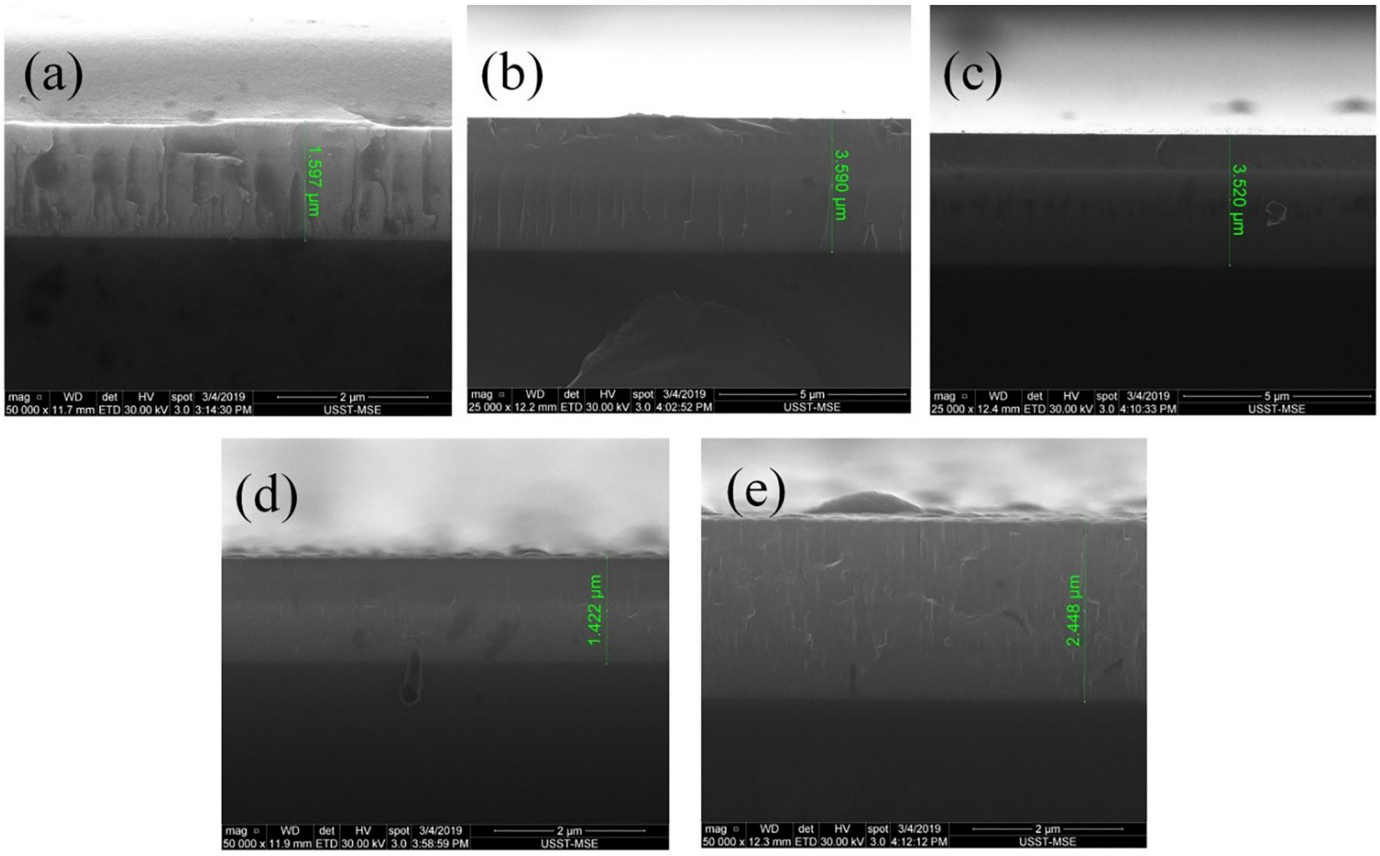

Fig. 5. SEM figures of the cross section of (AlCrTiZrMo)-Si_x-N thin films with different Si contents: (a) (AlCrTiZrMo)N; (b) (AlCrTiZrMo)-$Si_{2.3}$-N; (c) (AlCrTiZrMo)-$Si_{4.5}$-N; (d) (AlCrTiZrMo)-$Si_{5.9}$-N; (e) (AlCrTiZrMo)-$Si_{7.1}$-N.

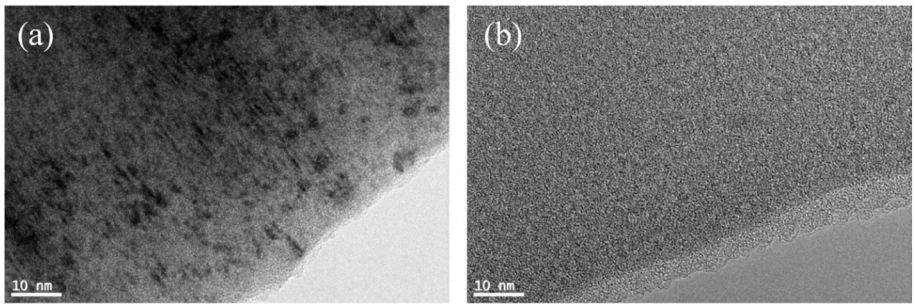

Fig. 6. Low-power HRTEM figure of film cross section: (a) (AlCrTiZrMo)N film (b) (AlCrTiZrMo)-$Si_{4.5}$-N film.

an amorphous phase. Therefore, according to HRTEM images, after the addition of Si elements, the HEA-nitride film formed a nanocomposite structure. From Fig. 7c, the (AlCrTiZrMo)N film has face-centered-cubic structures with a (200)-preferential orientation, while the (AlCrTiZrMo)-$Si_{4.5}$-N film in Fig. 7d has nanocrystalline and amorphous structures, which are consistent with the XRD and XPS analysis.

3.2. Effect of Si content on mechanical properties of AlCrTiZrMo-Si_x-N films

Fig. 8 shows the mechanical properties of AlCrTiZrMo-Si_x-N films with different silicon content. According to Fig. 8, the hardness and elastic modulus of (AlCrTiZrMo)N films without Si elements were 24.9 GPa and 292.8 GPa, respectively. With the addition of Si elements, the hardness and modulus of elasticity of the film have the same trend, which increases first and then decreases. On the whole, the mechanical properties of the film are improved after the addition of Si elements. Moreover, when the Si content is 4.5 at.%, the hardness and elastic modulus of the film reached the maximum, which were 28.5 GPa and 325.4GPa, respectively. This trend indicates that the addition of Si elements changes the microstructure of the film, which has a certain influence on the mechanical properties of the film.

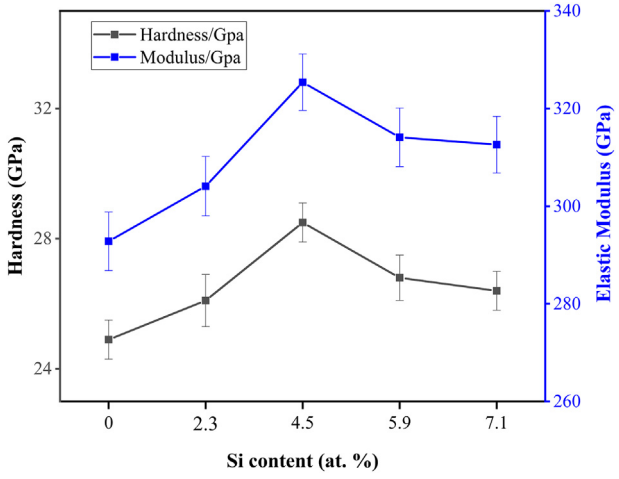

Fig. 8. Mechanical properties of AlCrTiZrMo-Si_x-N films with different Si contents.

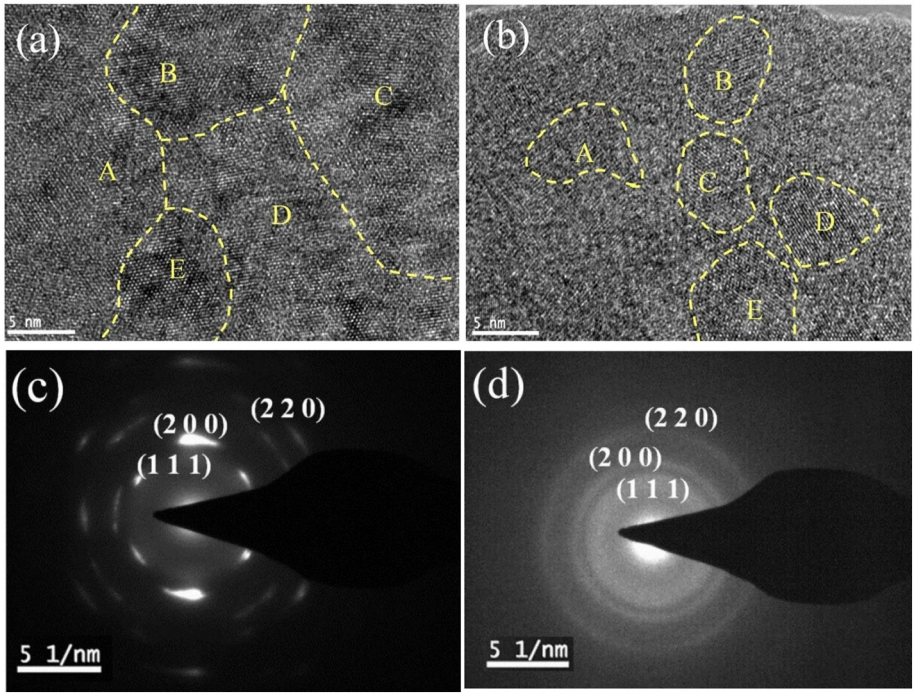

Fig. 7. High-power HRTEM images of cross sections of thin films and selected electron diffraction patterns: (a), (c) are (AlCrTiZrMo)N thin films; (b) and (d) are (AlCrTiZrMo)-$Si_{4.5}$-N thin films.

4. Discussion

4.1. Microstructures of the films

It can be seen from the Fig. 2 that when the silicon content increased from 0 to 2.3 at.%, the nitrogen element in the films varied lightly. This trend that the silicon atoms may dissolve in the solid-solution structure when the silicon content is low, the reason may be that the diameter of the silicon atoms is smaller than that of other elements in the film. Combined with the XRD pattern, with the increase of the silicon content to 4.5 at.%, the nitrogen element increases sharply, and the crystallinity drops, indicating that the microstructure of the film may be changing and forming nano microstructures.

A nanocomposite film, a three-dimensional network structure film, is formed from two or more materials and from the interfacial phase inclusions matrix phase, in which the interfacial phases are nanocrystalline or amorphous [12]. The formation of a nanocomposite membrane depends on the incompatibility between different material particles, which is a kind of composites composed of heterogeneous phases.

Due to the high-entropy effect of the HEAs films, solid-solution phases are prone to form in the films. Thus, the addition of silicon will affect the microstructures of HEAs films. Cheng et al. studied the effects of the silicon content on the structures and mechanical properties of (AlCrTaTiZr)-Si_x-N [48]. With the lower silicon content, the nitride film is still a simple NaCl FCC solid-solution structure, in which silicon atoms occupy the Na-lattice position like the other five metal elements. As the silicon content increases, the amorphous SiN_x in FCC solid nitrides is separated by thermodynamics. Then, the two phases permeate each other, and the amorphous segregation at grain boundary obviously inhibits the growth of nanocrystals. Therefore, only by adding the appropriate amount of silicon can the nanocomposite structure be formed in the thin film.

Combined with the above XRD and HRTEM images, it can be seen that the (AlCrTiZrMo)N thin film has a planar crystal structure, and the crystals are connected to each other. With the addition of the silicon content, the crystallinity of (AlCrTiZrMo)-Si_x-N decreases. This feature is due to the appearance of the interface phase, Si_3N_4, between crystal phases, which forms nanocomposite films. According to Prochazka's [49] research, the solubility of the α-Si_3N_4 phase in nitrides is limited, and thermodynamically-driven phase separation occurs in the deposition process, resulting in the separation of the crystalline phase and amorphous phase in the thin film, thus forming the nanocomposite structure, which is shown in Fig. 9.

4.2. The improvement of mechanical properties

With the addition of silicon, the hardness and elastic modulus of the film first increased and then decreased in Fig. 8. According to the solid-solution-hardening theory [50], the lattice distortion of nitride films can be caused by the addition of Si elements, improving the mechanical properties. The addition of Si elements causes the lattice distortion of nitride films to some extent. However, when the silicon content is high, the mechanical properties decrease, which indicates that the solid-solution strengthening is not the main factor to change the mechanical properties of nitride films, which may be attributed to the addition of silicon to change the nanometer microstructure of the film [51–54]. Based on the previous analysis, we are convinced that the nanocomposite structure is formed in the HEA-nitride film.

According to the atomic-size difference (2) [30], where $\bar{r} = \sum_{i=1}^{n} ciri$, ci and ri are the atomic percentage and atomic radius of the ith element. The constant, 100, is used to magnify the data for greater clarity. According to this formula, the lattice distortion caused by the incorporation of Si may have less effect on the grain size simply because the (AlCrTiZrMo)N films with different atomic sizes have higher lattice distortion. Therefore, the strengthening of fine crystals is not the main reason for the improvement of hardness and modulus of thin films.

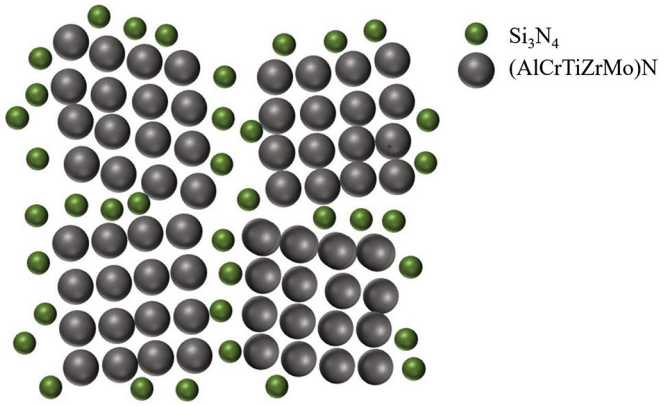

Fig. 9. Nanocomposite structure of the (AlCrTiZrMo)-Si_x-N films.

$$\text{Atomic}-\text{size difference} = 100\sqrt{\sum_{i=1}^{n} ci(1-ri/\bar{r})^2} \quad (2)$$

According to the Hall-Petch formula (3) [55], where H_0 is the intrinsic hardness of the (AlCrTiZrMo)N, d is the average grain size, and k_{HP} is the Hall-Petch coefficient of (AlCrTiZrMo)N. It can be seen from this trend that when the grain size is reduced, the fine-grain strengthening effect will be generated, and the hardness of the material will be improved. However, according to the previous analysis, after adding Si elements, the hardness of the film first increases and then decreases, which indicates that the grain size is not the main factor causing the change of mechanical properties of the film. Therefore, it is speculated that the formation of the nanocomposite structure is the main reason affecting the mechanical properties of thin films.

$$H = H_0 + K_{HP}d^{-1/2} \quad (3)$$

Combining the HRTEM image of the thin film shown in Fig. 6 with the strengthening mechanism of the nanocomposite film (nc-TiN/a-Si_3N_4 model) [41,56–58], it can be seen that after the addition of Si elements, many equiaxed crystals with nanometer sizes are formed in the film, which results in the dislocation unable to be generated or proliferated in the nanocrystalline grains. At the same time, the thickness of the amorphous boundary surface formed between nanocrystalline grains is small. Hence, the cracks are difficult to expand at the interface, resulting in the superhard effect of the thin film and the improvement of hardness and modulus. With the increase of the Si content, the interface phase increases, the grain becomes more refined, and the mechanical properties become better and reach the peak. However, Patscheider [56] showed that if the interface phase is too thick, the hardness of the nanocomposite membrane is mainly determined by the properties of the amorphous interface phase. In this experiment, with the further increase of the Si content (more than 4.5 at.%), there are too many amorphous boundary phases in the film and its thickness is large. At this time, the mechanical properties of the film are mainly determined by the properties of the amorphous boundary phase. Because SiN_x is relatively soft, the hardness of the film decreases. At the same time, due to the excessive phase of the amorphous boundary, the nanocomposite structure is damaged, and the crack can expand along the interface phase, which further degrades the mechanical properties of the thin film. Therefore, the incorporation of Si elements makes the mechanical properties of films increase first and then decrease. Compared with the films without Si elements, the mechanical properties of films mixed with Si elements are improved to a certain extent, which may be attributed to the fine-grain-strengthening effect caused by the grain refinement.

5. Conclusion

(1) The (AlCrTiZrMo)N film is a solid-solution phase with a single face-centered-cubic structure, (200)-preferential orientation, and its hardness and elastic modulus are 24.9 GPa and 292.8 GPa, respectively. With the addition of Si elements, the diffraction peak (200) of the (AlCrTiZrMo)-Si_x-N film disappeared, and the film presented an amorphous shape.

(2) (AlCrTiZrMo)N films were grown as columnar crystals, but the columnar crystal growth of (AlCrTiZrMo)-Si_x-N films was not obvious after the addition of Si elements. Moreover, the addition of Si elements can effectively refine the grain size of the film, thus forming nanocrystals with a size of about 5 nm, and a large number of amorphous boundary surfaces appear at the same time.

(3) With the addition of Si elements, the (AlCrTiZrMo)-Si_x-N film forms a nanocomposite structure, and the hardness of the film are improved. The strengthening mechanism can be explained by the nc-TiN/a-Si_3N_4 model. When the Si content was 4.5 at.%, the film had the highest hardness and elastic modulus were 28.5 GPa and 325.4 GPa, respectively. However, when the Si content exceeds 4.5 at.%, the hardness of the film will decrease. The main reason is that the film is softened due to the excessive amorphous boundary phase inside the film.

Credit Author Statement

WY designed the experiment and wrote the article.

WL, PL and KZ carried out the synthesis of (AlCrTiZrMo)-Si_x-N High-Entropy Alloy Nitride Films.

FM, XC, RF and PKL assisted the technical support for measurements (XRD, SEM, HRTEM, EPMA and nanoindention) as well as the data analysis. All authors read and approved the final manuscript.

Declaration of Competing Interest

The authors declare that they have no competing interests.

Acknowledgment

The present work was financially supported by the National Natural Science Foundation of China (No. 51971110, 51471110). RF and PKL very much appreciate the support of the National Science Foundation (DMR-1611180 and 1809640) with the program directors, Drs. J. Yang, G. Shiflet, and D. Farkas.

References

[1] R.J. Rodriguez, J.A. Garcia, A. Medrano, M. Rico, R. Sanchez, R. Martinez, C. Labrugere, M. Lahaye, A. Guette, Tribological behaviour of hard coatings deposited by arc-evaporation PVD, Vacuum. 67 (2002) 559–566.
[2] J.X. Deng, J.H. Liu, J.L. Zhao, W.L. Song, Wear mechanisms of PVD ZrN coated tools in machining, Int. J. Refract. Met. Hard Mater. 26 (2008) 164–172.
[3] K. Singh, P.K. Limaye, N.L. Soni, A.K. Grover, R.G. Agrawal, A.K. Suri, Wear studies of (Ti–Al)N coatings deposited by reactive magnetron sputtering, Wear. 258 (2005) 1813–1824.
[4] J. Gerth, U. Wiklund, The influence of metallic interlayers on the adhesion of PVD TiN coatings on high-speed steel, Wear. 264 (2008) 885–892.
[5] J. Jin, H.J. Duan, X.H. Li, The influence of plasma nitriding on microstructure and properties of CrN and CrNiN coatings on Ti6Al4V by magnetron sputtering, Vacuum. 136 (2017) 112–120.
[6] A.H. Liu, J.X. Deng, H.B. Cui, Y.Y. Chen, J. Zhao, Friction and wear properties of TiN, TiAlN, AlTiN and CrAlN PVD nitride coatings, Int. J. Refract. Met. Hard Mater. 31 (2012) 82–88.
[7] L. Wang, S.H. Zhang, Z. Chen, J.L. Li, M.X. Li, Influence of deposition parameters on hard Cr–Al–N coatings deposited by multi-arc ion plating, Appl. Surf. Sci. 258 (2012) 3629–3636.
[8] S. Fouvry, B. Wendler, T. Liskiewicz, M. Dudek, L. Kolodziejczyk, Fretting wear analysis of TiC/VC multilayered hard coatings: experiments and modelling approaches, Wear. 257 (2004) 641–653.
[9] M.L. Yin, C.X. Tian, Z.S. Wang, D.J. Fu, Influences of Bias voltage and target current on structure, microhardness and friction coefficient of multilayered TiAlN/CrN coatings synthesized by cathodic arc plasma deposition, Plasma Sci. Technol. 15 (2013) 582–585.
[10] J.W. Yeh, S.K. Chen, S.J. Lin, J.Y. Gan, T.S. Chin, T.T. Shun, C.H. Tsau, S.Y. Chang, Nano-structured high-entropy alloys with multiple principal elements: novel alloy Desigin concepts and outcomes, Adv. Eng. Mater. 6 (2004) 299–303.
[11] B. Cantor, I.T.H. Chang, P. Knight, A.J.B. Vincent, Microstructural development in equiatomic multicomponent alloys, Mater. Sci. Eng. A 375-377 (2004) 213–218.
[12] Y. Zhang, Y.J. Zhou, J.P. Lin, G.L. Chen, P.K. Liaw, Solid-solution phase formation rules for multi-component alloys, Adv. Eng. Mater. 10 (2008) 534–538.
[13] Y. Zhang, T.T. Zuo, Z. Tang, M.C. Gao, K.A. Dahmen, P.K. Liaw, Z.P. Lu, Microstructures and properties of high-entropy alloys, Prog. Mater. Sci. 61 (2014) 1–93.
[14] O.N. Senkov, G.B. Wilks, D.B. Miracle, C.P. Chuang, P.K. Liaw, Refractory high-entropy alloys, Intermetallics. 18 (2010) 1758–1765.
[15] H.W. Luan, Y. Shao, J.F. Li, W.L. Mao, Z.D. Han, C.L. Shao, K.F. Yao, Phase stabilities of high entropy alloys, Scr. Mater. 179 (2020) 40–44.
[16] W.D. Li, S.Y. Chen, P.K. Liaw, Discovery and design of fatigue-resistant high-entropy alloys, Scr. Mater. 187 (2020) 68–75.
[17] M. Seifi, D.Y. Li, Z. Yong, P.K. Liaw, J.J. Lewandowski, Fracture toughness and fatigue crack growth behavior of as-cast high-entropy alloys, Jom. 67 (2015) 2288–2295.
[18] M.A. Hemphill, T. Yuan, G.Y. Wang, J.W. Yeh, C.W. Tsai, A. Chuang, P.K. Liaw, Fatigue behavior of Al0.5CoCrCuFeNi high entropy alloys, Acta. Mater 60 (2012) 5723–5734.
[19] Z. Tang, T. Yuan, C.W. Tsai, J.W. Yeh, C.D. Lundin, P.K. Liaw, Fatigue behavior of a wrought Al0.5CoCrCuFeNi two-phase high-entropy alloy, Acta. Mater 99 (2015) 247–258.
[20] K. Liu, S.S. Nene, M. Frank, S. Sinha, R.S. Mishra, Metastability-assisted fatigue behavior in a friction stir processed dual-phase high entropy alloy, Mater. Res. Lett. 6 (2018) 613–619.
[21] K.V.S. Thurston, B. Gludovatz, A. Hohenwarter, G. Laplanche, E.P. George, R.O. Ritchie, Effect of temperature on the fatigue-crack growth behavior of the high-entropy alloy CrMnFeCoNi, Intermetallics. 88 (2017) 65–72.
[22] B. Gludovatz, A. Hohenwarter, D. Catoor, E.H. Chang, E.P. George, R.O. Ritchie, A fracture-resistant high-entropy alloy for cryogenic applications, Science. 345 (2014) 1153–1158.
[23] Y. Shi, B. Yang, P.K. Liaw, Corrosion-resistant high-entropy alloys: a review, Metals. 7 (2017) 43.
[24] Y.Z. Shi, B. Yang, X. Xie, J. Brechtl, K.A. Dahmen, P.K. Liaw, Corrosion of AlCoCrFeNi high-entropy alloys: Al-content and potential scan-rate dependent pitting behavior, Corros. Sci. 119 (2017) 33–45.
[25] Y. Zhang, G.M. Stocks, K. Jin, C. Lu, H. Bei, B.C. Sales, L. Wang, L.K. Beland, R.E. Stoller, G.D. Samolyuk, M. Caro, A. Caro, W.J. Weber, Influence of chemical disorder on energy dissipation and defect evolution in concentrated solid solution alloys, Nat. Commun. 6 (2015) 8736.
[26] N.A.P. Kiran Kumar, C. Li, K.J. Leonard, H. Bei, S.J. Zinkle, Microstructural stability and mechanical behavior of FeNiMnCr high entropy alloy under ion irradiation, Acta Mater. 113 (2016) 230–244.
[27] F.V. Rohr, M.J. Winiarski, J. Tao, T. Klimczuk, R.J. Cava, Effect of electron count and chemical complexity in the ta-Nb-Hf-Zr-Ti high-entropy alloy superconductor, Proc. Natl. Acad. Sci. U. S. A. 113 (2016) E7144–E7150.
[28] W. Li, P. Liu, P.K. Liaw, Microstructures and properties of high-entropy alloy films and coatings: a review, Mater. Res. Lett. 6 (2018) 199–229.
[29] K.M. Youssef, A.J. Zaddach, C.N. Niu, D.L. Irving, C.C. Koch, A novel low-density, high-hardness, high-entropy alloy with close-packed single-phase nanocrystalline structures, Mater. Res. Lett. 3 (2014) 95–99.
[30] D.C. Tsai, Z.C. Chang, B.H. Kuo, S.Y. Chang, F.S. Shieu, Effects of silicon content on the structure and properties of (AlCrMoTaTi)N coatings by reactive magnetron sputtering, J. Alloys Compd. 616 (2014) 646–651.
[31] E. Lewin, Multi-component and high-entropy nitride coatings-a promising field in need of a novel approach, J. Appl. Phys. 127 (2020) 160901.
[32] T.K. Chen, T.T. Shun, J.W. Yeh, M.S. Wong, Nanostructured nitride films of multi-element high-entropy alloys by reactive DC sputtering, Surf. Coat. Technol. 188-189 (2004) 193–200.
[33] P.P. Cui, W. Li, P. Liu, K. Zhang, F.C. Ma, X.H. Chen, R. Feng, P.K. Liaw, Effects of nitrogen content on microstructures and mechanical properties of (AlCrTiZrHf)N high-entropy alloy nitride films, J. Alloys Compd. 834 (2020) 155063.
[34] K.H. Cheng, C.H. Weng, C.H. Lai, S.J. Lin, Study on adhesion and wear resistance of multi-element (AlCrTaTiZr)N coatings, Thin Solid Films 517 (2009) 4989–4993.
[35] C.H. Lai, K.H. Cheng, S.J. Lin, J.W. Yeh, Mechanical and tribological properties of multi-element (AlCrTaTiZr)N coatings, Surf. Coat. Technol. 202 (2008) 3732–3738.
[36] C.H. Lai, M.H. Tsai, S.J. Lin, J.W. Yeh, Influence of substrate temperature on structure and mechanical, properties of multi-element (AlCrTaTiZr)N coatings, Surf. Coat. Technol. 201 (2007) 6993–6998.
[37] N. Tüten, D. Canadinc, A. Motallebzadeh, B. Bal, Microstructure and tribological properties of TiTaHfNbZr high entropy alloy coatings deposited on Ti6Al4V substrates, Intermetallics. 105 (2019) 99–106.
[38] V. Braic, A. Vladescu, M. Balaceanu, C.R. Luculescu, M. Braic, Nanostructured multi-element (TiZrNbHfTa)N and (TiZrNbHfTa)C hard coatings, Surf. Coat. Technol. 211 (2012) 117–121.
[39] J. Musil, Z. Čiperová, R. Čerstvý, S. Haviar, Flexible hard (Zr, Si) alloy films prepared by magnetron sputtering, Thin Solid Films 688 (2019) 1312276.
[40] S.Z. Li, Y.L. Shi, H.R. Peng, Ti-Si-N films prepared by plasma-enhanced chemical vapor deposition, Plasma Chem. Plasma Process. 12 (1991) 287–297.
[41] S. Vepřek, S. Reiprich, S.Z. Li, Superhard nanocrystalline composite materials: the TiN/Si_3N_4 system, Appl. Phys. Lett. 66 (1995) 2640–2642.

[42] J. Shi, C.M. Muders, A. Kumar, X. Jiang, Z.L. Pei, J. Gong, C. Sun, Study on nanocomposite Ti–Al–Si–cu–N films with various Si contents deposited by cathodic vacuum arc ion plating, Appl. Surf. Sci. 258 (2012) 9642–9649.
[43] J.R. Niu, W. Li, P. Liu, K. Zhang, F.C. Ma, X.H. Chen, R. Feng, P.K. Liaw, Effects of silicon content on the microstructures and mechanical properties of (AlCrTiZrV)-six-N high-entropy alloy films, Entropy. 21 (2019) 75.
[44] W.C. Oliver, G.M. Pharr, An improved technique for determining hardness and elastic modulus using load and displacement sensing indentation experiments, J. Mater. Res. 7 (1992) 1564–1583.
[45] R. Chen, Z.B. Cai, J.B. Pu, Z.X. Lu, S.Y. Chen, S.J. Zheng, C. Zeng, Effects of nitriding on the microstructure and properties of VAlTiCrMo high-entropy alloy coatings by sputtering technique, J. Alloys Compd. 827 (2020) 153836.
[46] Y. Dong, Y.P. Lu, L. Jiang, T.M. Wang, T.J. Li, Effects of electro-negativity on the stability of topologically close-packed phase in high entropy alloys, Intermetallics. 52 (2014) 105–109.
[47] S.P. Wang, J. Xu, TiZrNbTa-Mo high-entropy alloys: Dependence of microstructure and mechanical properties on Mo concentration and modeling of solid solution strengthening, Intermetallics 95 (2018) 59–72.
[48] K.H. Cheng, C.W. Tsai, S.J. Lin, J.W. Yeh, Effects of silicon content on the structure and mechanical properties of (AlCrTaTiZr)–six–N coatings by reactive RF magnetron sputtering, J. Phys. D. Appl. Phys. 44 (2011) 205405.
[49] J. Procházka, P. Karvánková, M.G.J. Vepřek-Heijman, S. Vepřek, Conditions required for achieving superhardness of ≥45GPa in nc-TiN/a-Si_3N_4 nanocomposites, Mater. Sci. Eng. A 384 (2004) 102–116.
[50] J.L. He, C.K. Chen, M.H. Hon, Microstructure and properties of Ti-Si-N films prepared by plasma-enhanced chemical vapor deposition, Mater. Chem. Phys. 44 (1996) 9–16.
[51] L.C. Qiu, Y. Du, S.Q. Wang, K. Li, L. Yin, L.Y. Wu, Z.Q. Zhong, L. Albir, Mechanical properties and oxidation resistance of chemically vapor deposited TiSiN nanocomposite coating with thermodynamically designed compositions, Int. J. Refract. Met. Hard Mater. 80 (2019) 30–39.
[52] Y.X. Chen, S. Zhu, X.M. Wang, B.J. Yang, G.F. Han, L. Qiu, Microstructure evolution and strengthening mechanism of Al0.4CoCu0.6NiSix (x=0–0.2) high entropy alloys prepared by vacuum arc melting and copper injection fast solidification, Vacuum 150 (2018) 84–95.
[53] A. Kumar, P. Dhekne, A.K. Swarnakar, M.K. Chopkar, Analysis of Si addition on phase formation in AlCoCrCuFeNiSix high entropy alloys, Mater. Lett. 188 (2017) 73–76.
[54] Z.R. Geng, H.X. Wang, C.B. Wang, L.P. Wang, G.G. Zhang, Effect of Si content on the tribological properties of CrSiN films in air and water environments, Tribol. Int. 79 (2014) 140–150.
[55] W.H. Liu, Y. Wu, J.Y. He, T.G. Nieh, Z.P. Lu, Grain growth and the hall–Petch relationship in a high-entropy FeCrNiCoMn alloy, Scr. Mater. 68 (2013) 526–529.
[56] J. Patscheider, T. Zehnder, M. Diserens, Structure-performance relations in nanocomposite coatings, Surf. Coat. Tech. 146-147 (2001) 201–208.
[57] S. Veprek, R.F. Zhang, M.G.J. Veprek Heijman, S.H. Sheng, A.S. Argon, Superhard nanocomposites: origin of hardness enhancement, properties and applications, Surf. Coat. Technol. 204 (2010) 1898–1906.
[58] S. Veprek, A. Niederhofer, K. Moto, T. Bolom, H.D. Mannling, P. Nesladek, G. Dollinger, A. Bergmaier, Composition, nanostructure and origin of the ultrahardness in nc-TiN/a-Si_3N_4/a- and nc-$TiSi_2$ nanocomposites with HV=80 to ≥105 GPa, Surf. Coat. Tech. 133-134 (2000) 152–159.